CHINESE OPTICS LETTERS

Vol. 22, No. 2 | February 2024

Generation of visible Raman operation laser by a fiber electro-optical modulator feedback loop

Rui-Rui Li (李睿睿)[1,2], Wei-Ran Ye (叶蔚然)[1,2], Yi-Long Chen (陈一龙)[1,2], Shu-Qian Chen (陈树谦)[1,2], Wen-Hao Qi (亓文昊)[1,2], Jin-Ming Cui (崔金明)[1,2,3], Yun-Feng Huang (黄运锋)[1,2,3*], Chuan-Feng Li (李传锋)[1,2,3], and Guang-Can Guo (郭光灿)[1,2,3]

[1] CAS Key Laboratory of Quantum Information, University of Science and Technology of China, Hefei 230026, China

[2] CAS Center for Excellence in Quantum Information and Quantum Physics, University of Science and Technology of China, Hefei 230026, China

[3] Hefei National Laboratory, University of Science and Technology of China, Hefei 230088, China

*Corresponding author: hyf@ustc.edu.cn

Received August 23, 2023 | Accepted October 9, 2023 | Posted Online February 22, 2024

Phase-coherent multi-tone lasers play a critical role in atomic, molecular, and optical physics. Among them, the Raman opeartion laser for manipulating atomic hyperfine qubits requires gigahertz bandwidth and low phase noise to retain long-term coherence. Raman operation lasers generated by directly modulated and frequency-multipled infrared lasers are compact and stable but lack feedback control to actively suppress the phase noise, which limits their performance in practical applications. In this work, we employ a fiber electro-optical modulator driven by a voltage-controlled oscillator (VCO) to modulate a monochromatic laser and employ a second-harmonic generation process to convert it to the visible domain, where the beat note of the Raman operation laser is stabilized by controlling the output frequency of VCO with a digital phase-locked loop (PLL). The low-frequency phase noise is effectively suppressed compared to the scheme without active feedback and it reaches −80 dBc/Hz@5 kHz with a 20 kHz loop bandwidth. Furthermore, this compact and robust scheme effectively reduces the system's complexity and cost, which is promising for extensive application in atomic, molecular, and optical physics.

Keywords: phase-coherent laser; quantum information; trapped ion; stimulated Raman transition; phase-locked loop.
DOI: 10.3788/COL202422.022702

1. Introduction

Phase-coherent multi-tone lasers play a crucial role in the fields of modern information technology, e.g., optical microwave generation[1–4], and atomic physics, e.g. atomic clocks[5–7], quantum precision measurement[8–13], and qubits manipulation[14–18]. Among them, the stimulated Raman transition is widely used to manipulate atomic hyperfine qubits[19,20], and the Raman operation laser typically requires optical fields with gigahertz-level frequency difference to match the atomic energy levels. Furthermore, to obtain a long-term coherent time, the phase noise of the Raman operation laser has to be as low as possible. Plenty of technologies, such as optical phase locking (OPL)[21–25] and directly modulated lasers[26–29], have been developed to generate phase-coherent optical fields with gigahertz frequency difference for Raman operation. Among these technologies, OPL typically necessitates two separate laser sources and complex electrical feedback controls and suffers from poor robustness and high system complexity.

As a comparison, directly modulated lasers, which apply a low noise driving signal on acousto- or electro-optical modulators (AOMs or EOMs) to directly diffract a single laser, feature quite good stability and compact structures. The low bandwidth of AOMs and the narrow tuning range of resonant EOMs limit the performance of the directly modulated laser system. However, fiber EOMs (FEOMs), which possess a gigahertz bandwidth and wide tuning range, are now widely used in directly modulated lasers. Most of opeartion wavelengths of FEOMs are infrared or telecom (1550 nm), which are far away from the D_1 lines of the atomic qubits. To acquire considerable Rabi frequency, it necessitates a second-harmonic generation (SHG) process to down-convert operation wavelengths of FEOMs to wavelengths closer to the D_1 lines. In such systems, despite directly-modulated lasers conserving the phase noise performance of the driving signal, it degenerates with the external perturbations, e.g., the perturbations from the SHG process, because of the lack of active suppression for the phase noise. Thus, an active phase noise suppression subsystem is crucial for enhancing the performance of directly-modulated lasers.

In this work, we demonstrate a compact, robust, and low phase noise scheme that utilizes an FEOM feedback loop to

generate multi-tone lasers and suppress the phase noise. We utilize an FEOM driven by a voltage-controlled oscillator (VCO) to modulate a monochromatic 1064 nm laser to generate the desired sidebands. The frequency difference between sidebands equals the hyperfine splitting of the $^{171}Yb^{+}$ qubit[30]. Then, the modulated laser is converted to a 532-nm three-tone laser via second harmonic generation (SHG) conversion. After SHG conversion, we then inject the 1064-nm laser into a fast photoelectric detector (FPD) to acquire the beat note signal (BNS). A digital PLL is employed to control the output frequency of the VCO to narrow the linewidth of the BNS (~1 Hz) and suppress the phase noise. We find that the phase noise of our scheme is lower than that of the case without feedback control in the low-frequency domain, and it reaches −80 dBc/Hz@5 kHz with a loop bandwidth of 20 kHz. Moreover, by replacing the luxury and bulky commercial signal generator with inexpensive and miniature devices, our scheme significantly reduces the system's complexity and cost. Our scheme can rebuild a closed loop within 150 μs when encountering a hopping of reference signal, indicating its frequency turning agility. Those features make this scheme promising for application in some extreme environments, e.g., atomic clocks in space and portable atomic gravimeters transported by trucks.

2. Experimental Setup

The schematic of our experimental setup is shown in Fig. 1(a). Here, we adopt a master oscillator power amplifier (MOPA) configuration, which only contains a single laser to simplify the system architecture and improve the maintainability. A 1064 nm monochromatic laser (ML, Koheras BASIK Y10, NKT Photonics, Japan) that only outputs one frequency component is used as a seed laser. To narrow the linewidth and stabilize the long-term frequency drift of the ML, we lock the frequency of the ML to an ultra-stable Fabry–Pérot cavity with Pound–Drever–Hall technology[31]. The optical field of the ML is written as

$$E_{\mathrm{ML}} = E_0 e^{j\omega_0 t}, \tag{1}$$

where ω_0 is the frequency of the ML.

Then, the output beam of the ML is sent into an FEOM (iXblue, NIR-MX-LN-20, France) driven by the VCO (Mini-Circuits, ROS-6520C-119+, USA), of which the tuning range is 6250 MHz to 6630 MHz, to generate multi-tone lasers. In our practical application shown in this work, we adopt a fiber Mach–Zehnder modulator that operates at carrier-suppression and double-sideband (CS-DSB) modulation to suppress redundant frequency components generated by EOM modulation, as we described in detail in Ref. [29]. One can also adopt a phase modulator as a substitute of the Mach-Zehnder modulator since they have the same principle that generates such phase-coherent multi-tone lasers. In our case, we lock the frequency of the BNS to the hyperfine ground state splitting of the $^{171}Yb^{+}$ qubit, i.e., $|0\rangle \equiv {}^2S_{1/2}|F=0, m_F=0\rangle$ and $|1\rangle \equiv {}^2S_{1/2}|F=1, m_F=0\rangle$. The hyperfine ground state splitting is 12.64 GHz, and we denote it as ω_{HF}. Here, the Raman operation laser is the 532-nm visible laser with 248 THz detuning from the $^2P_{1/2}$ state. The relevant energy levels are shown in Fig. 1(b). Hence, the driving frequency of the FEOM (or the output frequency of the VCO), which is denoted as ω_{E}, has to be locked to half of the ω_{HF}. The optical fields following the FEOM is written as

$$E_{\mathrm{FEOM}} = E_0 e^{j(\omega-\omega_{\mathrm{E}})t} + E_0 e^{j(\omega+\omega_{\mathrm{E}})t}. \tag{2}$$

Here, we assume that the amplitudes of the optical fields is normalized.

Multi-tone lasers are subsequently amplified by an Yb-doped fiber amplifier (YDFA, Precilasers, YDFA-SF-1064-8 W-CW, China), and the maximum output power of the YDFA is

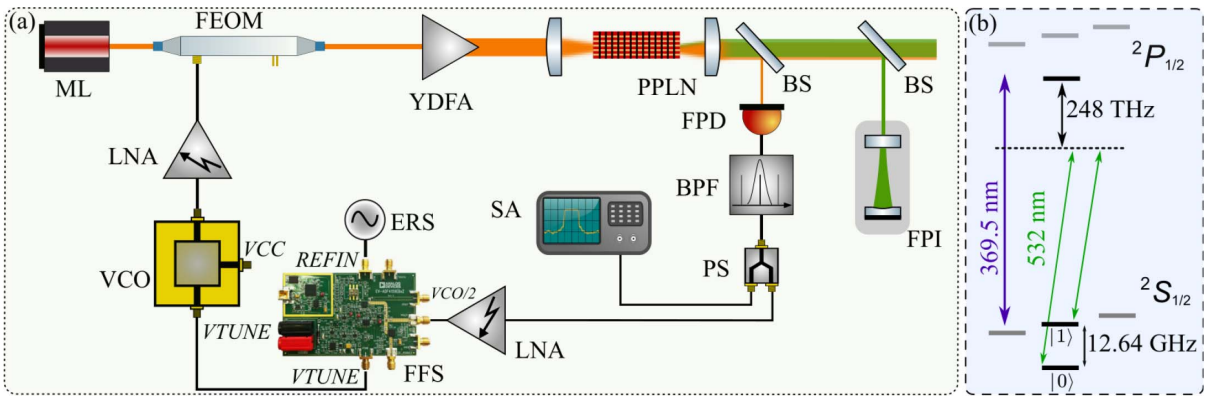

Fig. 1. (a) Schematic of the experimental setup. Some concerned ports of the FFS chip and the VCO chip are marked by italics in the figure. (b) Energy level schematic of the $^{171}Yb^{+}$ qubits. The energy levels associated with the stimulated Raman transition (SRT). Here, we utilize two 532 nm optical fields with a frequency difference of 12.64 GHz to implement the SRT. The transition wavelength for Doppler cooling is 369.5 nm. ML, monochromatic laser; FEOM, fiber electro-optic modulator; YDFA, ytterbium-doped fiber amplifier; BS, beam splitter; PPLN, periodically polarized lithium niobate; LNA, low-noise amplifier; FPD, fast photoelectric detector; VCO, voltage-controlled oscillator; ERS, external reference signal; PS, power splitter; SA, spectrum analyzer; FFS, fractional-N frequency synthesizer; FPI, Fabry–Pérot interferometer.

8 W. The amplified laser is focused by a lens and then sent to a PPLN crystal where the second-harmonic generation (SHG) occurs. Here, the SHG process converts the laser from the infrared domain to the visible domain to obtain a higher effective Rabi frequency. After SHG conversion, part of the 1064-nm lasers have been converted to 532-nm lasers, the rest of them are emitted from the PPLN crystal and are sampled by a beam splitter (BS). The sample 1064 nm laser is sent to a fast photoelectric detector (FPD) with a sensitivity of 0.7 A/W@1550 nm and a bandwidth of 20 GHz (Keyang Photonics, KY-APRM-20G, China). The power of the incident laser should be close to the saturation intensity of the FPD (500 μW@1550 nm) to acquire a signal-to-noise ratio as high as possible, given that the dark current of this FPD is fixed at 50 nA. The output signal of the FPD is written as

$$\begin{aligned} I_{\mathrm{FPD}} &\propto |E_{\mathrm{FEOM}}|^2 \\ &= E_0^2[1+\cos(2\omega_{\mathrm{E}}t)]. \end{aligned} \tag{3}$$

The direct current (DC) component and high frequency components in the output signal of the FPD are filtered by a bandpass filter (BPL, A-INFO, China, 12.55 GHz to 13.30 GHz). Subsequently, a power divider splits the BNS into two portions. One is sent to a spectrum analyzer (SA) to monitor the spectrum of the BNS and the performance of the phase-locked system. Meanwhile, the other portion is sent to a broad-bandwidth and low-noise amplifier (Mini-Circuits, ZVA-213-S+, USA, 0.8 GHz to 21 GHz). The amplified BNS is written as

$$I_{\mathrm{BN}} \propto \cos(2\omega_{\mathrm{E}}t). \tag{4}$$

For convenience, we omit the phase term of the BNS.

The BNS is sent to a fractional-N frequency synthesizer (FFS) chip (ADI, ADF4159, USA) of which the output frequency is up to 13 GHz. The ADF4159 consists of a low-noise digital frequency and phase discriminator (PFD), a precision charge pump, and a programmable reference divider. The input RF signal, i.e., the BNS, is connected to the VCO/2 port while an ERS from a rubidium frequency standard (SRS, FS725, USA) is connected to the REFIN port. The ERS, of which the frequency is 10 MHz, possesses an ultra-low phase noise of −130 dBc/Hz@10 Hz, a temperature stability of $\pm 1\times10^{-10}$ (+10°C to +40°C), and an aging rate of 5×10^{-10}/year to satisfy the strict requirements of the PLL.

The chip digitally divides the BNS by a factor of N (depending on the frequency of the ERS, the R, and the locking frequency) and the ERS by a factor of R (1 in our scheme) and then sends them to the PFD, where the frequencies and phases of both divided signals are being compared. The phase error signal generated by the PFD is subsequently sent to a predefined low-pass loop filter and transferred into a control voltage via the precision charge pump. The control voltage signal is written as

$$U_{\mathrm{VCO}} = G\cdot\sin\left[\left(\frac{2\omega_{\mathrm{E}}}{N}-\omega_{\mathrm{ERS}}\right)t+\Delta\theta\right], \tag{5}$$

where G represents the gain coefficient of the loop, ω_{ERS} is the frequency of the ERS given that R is set to 1, and $\Delta\theta$ is the phase difference between the BNS and the ERS. The control voltage, which is output from the VTUNE port of the FFS, is connected to the VTUNE port of the VCO to control its output frequency and can be written as

$$\omega_{\mathrm{E}} = \omega_{\mathrm{HF}}/2 + K\cdot U_{\mathrm{VCO}}, \tag{6}$$

where K is the voltage sensitivity of the VCO. The frequency range of the VCO is 6.25 GHz to 6.63 GHz, corresponding to the control voltage range from 0 V to 4.5 V and voltage sensitivity of 77 MHz/V to 92 MHz/V.

In the case that locking frequency equals the ω_{HF}, we have

$$N = \frac{\omega_{\mathrm{HF}}}{\omega_{\mathrm{ERS}}/R}. \tag{7}$$

Thus, Eq. (5) turns to zero and the output frequency of the VCO is locked at $\omega_{\mathrm{HF}}/2$ when the phase-locked loop is established.

The output signal of the VCO is amplified by another LNA to ensure that the FEOM outputs sufficient laser power that exceeds the threshold of the YDFA. The low-pass loop filter is designed to filter out the high-frequency noise that existed in the control voltage. A high loop bandwidth will introduce high-frequency noise and degrade the performance of the PLL, while a low loop bandwidth will limit the response speed of the system. Therefore, we design a loop filter with a bandwidth of 20 kHz as a trade-off for the above conditions.

Two LNAs, the VCO, the FPD, and the FFS are all powered by isolated linear power supplies to avoid the detrimental effect of electrical noise.

3. System Characterization

We connect the monitor port of the PD to an SA to acquire the power density spectrum of the BNS. Figure 2(a) shows a comparison between the spectrum of the BNS when the system is free running (red line) and the loop is closed (black line), respectively. For both spectra, the resolution bandwidth (RBW) and the video bandwidth (VBW) of the SA are set to 10 Hz and 10 Hz, respectively. The center frequency of the BNS equals the ω_{HF} when the loop is closed. There are two significant differences between these two spectra.

In the case of free running system, the BNS has a wide line width while the phase-locked loop successfully narrows the linewidth. Moreover, in the case of a closed loop, a low and wide peak appears at the offset frequency of near 20 kHz (matches well with our design) in the spectrum. This mainly results from the high gain within the bandwidth of the loop filter. Those undesired peaks appearing at frequencies 27 kHz (black line) and 37 kHz (red line) may be caused by the unquenched noise from the linear power supply. Figure 2(b) shows an expanded view of the BNS when the loop is closed. In this case, the RBW is set to 1 Hz and the VBW is set to 10 Hz. We calculate

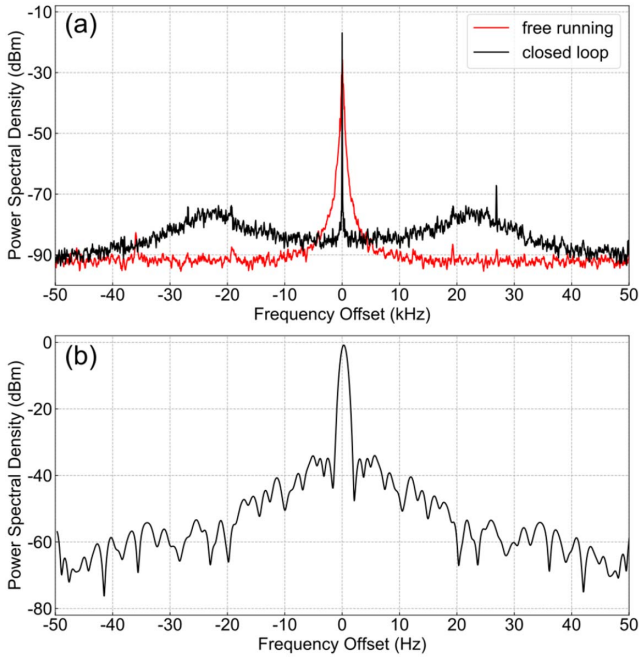

Fig. 2. (a) Comparison between the spectrum of the BNS when the system is free running and the loop is closed. The frequency span is set to 100 kHz, and the RBW and the VBW are both set to 10 Hz. (b) Expanded view of the BNS when the loop is closed. The frequency span is set to 100 Hz. The RBW is set to 1 Hz, and the VBW is set to 10 Hz.

the 3 dB linewidth of the BNS when the loop is close to about 1 Hz.

To characterize the phase noise performance of the phase-locked system, we replace the SA with a phase-noise analyzer to measure the phase noise of the BNS in the case of the FEOM driven by the FFS. As a comparison, we also measure the phase noise of the BNS in the case of the FEOM directly driven by a commercial signal generator (Rohde & Schwarz, SMB100A, Germany), as in our previous scheme. The measured phase noises are shown in Fig. 3. The phase noise of the BNS, in the case that the FEOM is driven by the FFS, is lower than that in the case of the FEOM driven by the SMB100A in the range of 1 Hz to 100 Hz. The phase noise reaches a flat floor of −80 dBc/Hz in the offset frequency range of 100 Hz to 5 kHz, and then it bumps up to −65 dBc/Hz at 20 kHz, which is the bandwidth of the loop filter. The phase noise is below −100 dBc/Hz when the offset frequency is higher than 100 kHz.

Typically, within the bandwidth of the loop filter, the phase noise is related to the ERS, the factor N, and the charge pump. Given that our ERS has ultra-low phase noise, the phase noise is dominated by the latter two. On the one hand, the phase noise can be suppressed by lowering the factor N, which needs to increase the frequency of the ERS due to the fixed locking frequency of the closed loop. On the other hand, the current noise of the charge pump will deteriorate the phase noise. Thus, employing a low-noise power supply for the charge pump helps to obtain a better performance of the phase noise. In addition,

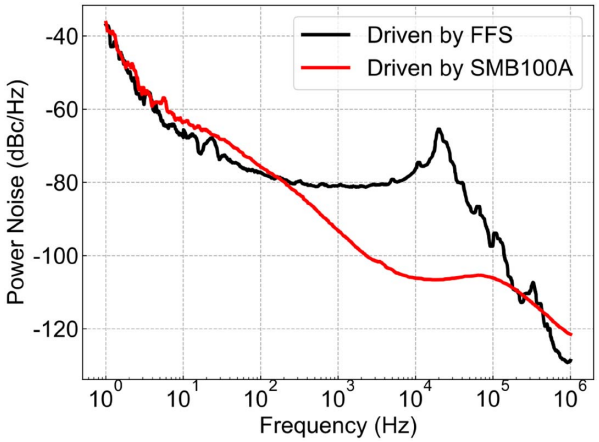

Fig. 3. Phase noise comparison between our scheme (when the loop is closed) and the scheme when the FEOM is directly driven by a commercial signal generator. The phase noise is measured by a phase noise analyzer rather than an SA.

electrical shielding added to different devices also helps to improve the performance of the phase noise.

The dynamic performance of the PLL is crucial to flexibly tune the frequency gap between the multi-tone lasers, which has the potential to be applied to manipulating multiple species of ion qubits. We measure the re-locking time of the system to characterize its dynamic performance, which refers to the time interval the PLL takes to recover a locked state after a sudden change of locking frequency. Initially, the system is stably locked at ω_{HF}, which is 12.64 GHz. The voltage of the VTUNE port is 1.24 V, corresponding to the output frequency of 6.32 GHz. At the time $t = 0$, we suddenly apply a frequency hopping to shift the locking frequency to 12.74 GHz. The voltage change of the VTUNE port with time is recorded by an oscilloscope, as shown in Fig. 4.

When the locking frequency is increased, the voltage of the VTUNE port is simultaneously increased to track the locking

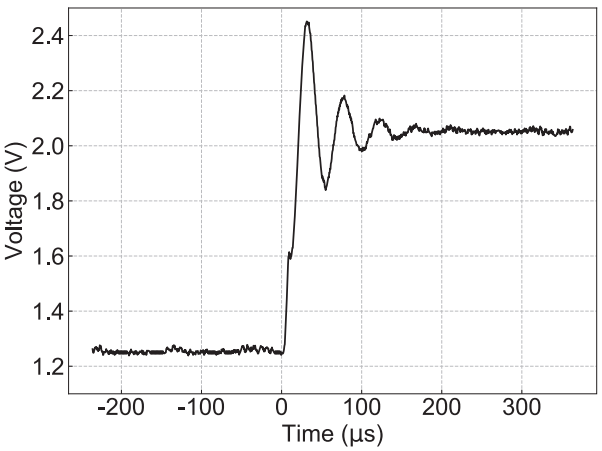

Fig. 4. Dynamic performance of the PLL system. The locking frequency changes at the time t = 0. The voltage change of the VTUNE port with time is recorded by an oscilloscope. The rising time and the re-locking time are about 20 μs and 150 μs, respectively, according to the measured result.

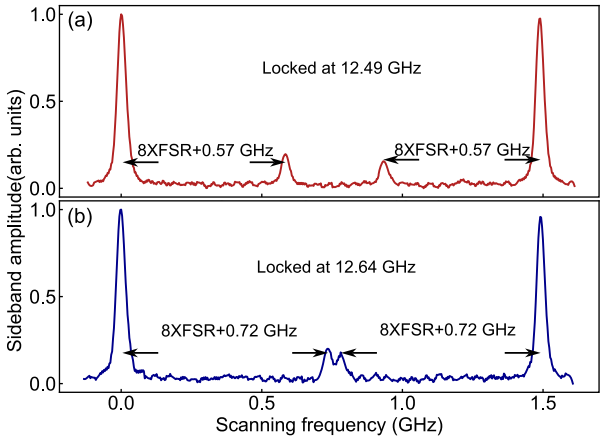

Fig. 5. Sideband spectra of the 532-nm laser measured with an FPI. When the driving frequency of the FEOM changes, the sidebands appear at the corresponding positions.

frequency, and the rise time is 20 μs. It takes the PLL about 150 μs to relock after a feedback process, which is indicated by the damped oscillation at the beginning of the waveform. By widening the bandwidth of the PLL, we can obtain a shorter re-locking time.

For our application, for manipulating the quantum state of the $^{171}Yb^{+}$ qubit via SRT, the phase-locked 1064-nm laser is sent to a PPLN crystal to generate a 532-nm multi-tone laser. The optical field of the 532-nm laser is written as

$$E_{532} = A_1 \cdot e^{j(2\omega_0 - 2\omega_E)t} + A_0 \cdot e^{j2\omega_0 t} + A_1 \cdot e^{j(2\omega_0 + 2\omega_E)t}, \quad (8)$$

where A_0 and A_1 denote the amplitudes of different sidebands. The frequency difference between adjacent sidebands equals the hyperfine splitting of the $^{171}Yb^{+}$ qubit. We utilize a BS to steer a small portion of the 532-nm laser to a scanning FPI (Thorlabs, SA200-3B, USA) to characterize its frequency components. The 532-nm Raman operation laser has to possess phase-coherent components between which the frequency difference equals ω_{HF}.

When the PLL is locked at the frequency of 12.49 GHz and 12.64 GHz (which is ω_{HF}), the corresponding sideband spectra of the 532-nm laser are recorded and are shown in Figs. 5(a) and 5(b), respectively. It is worth noting that the free spectral range (FSR) of the FPI is 1.49 GHz. In Fig. 5(a), the frequency difference between the sidebands with lower amplitude and the sideband with maximum amplitude is $8 \times \mathrm{FSR} + 0.57$ GHz, which matches the reference frequency of 12.49 GHz. When the reference frequency switches to 12.64 GHz, the position of the sidebands in 532-nm laser changes correspondingly. The result indicates that the generated multi-tone 532-nm laser can manipulate the $^{171}Yb^{+}$ qubit via SRT.

4. Conclusion and Outlook

To conclude, we demonstrate a scheme that employs an FEOM feedback loop to generate multi-tone lasers and suppress the phase noise. In this scheme, a monochromatic laser is modulated by an FEOM driven by the VCO to generate sidebands with gigahertz frequency difference. The modulated laser is amplified by a YDFA and converted to a visible Raman operation laser via SHG. The BNS is then stabilized by a digital feedback loop to suppress the phase noise caused by external perturbations. The phase noise of our scheme is up to 7.4 dB lower than that of the scheme in which the FEOM is driven by a commercial signal generator in a low-frequency domain. Distinct from the OPL schemes and direct modulation schemes, our scheme only requires a single laser and replaces the commercial signal generator with easily available and inexpensive devices, which significantly reduces the system's complexity and cost.

Acknowledgements

This work was supported by the National Key Research and Development Program of China (No. 2017YFA0304100), National Natural Science Foundation of China (Nos. 11774335, 11734015, and 12204455), the Key Research Program of Frontier Sciences, CAS (No. QYZDY-SSWSLH003), and Innovation Program for Quantum Science and Technology (Nos. 2021ZD0301604 and 2021ZD0301200). We thank the USTC Center for Micro and Nanoscale Research and Fabrication for technically supporting the fabrication of optical components.

References

1. J. Yao, "Microwave photonics," J. Lightwave Technol. **27**, 314 (2009).
2. T. Uehara, K. Tsuji, K. Hagiwara, *et al.*, "Optical beat-note frequency stabilization between two lasers using a radio frequency interferometer in the gigahertz frequency band," Opt. Eng. **53**, 124109 (2014).
3. W. Ren, J. Sun, P. Hou, *et al.*, "Direct phase control method for binary phase-shift keying space coherent laser communication," Chin. Opt. Lett. **20**, 060601 (2022).
4. X. Liu, J. Hu, Q. Bian, *et al.*, "Recent advances in optical injection locking for visible light communication applications," Photonics **10**, 291 (2023).
5. J. Vanier, "Atomic clocks based on coherent population trapping: a review," Appl. Phys. B **81**, 421 (2005).
6. Z. Wang, "Review of chip-scale atomic clocks based on coherent population trapping," Chinese Phys. B **23**, 030601 (2014).
7. S. Knappe, V. Shah, P. D. D. Schwindt, *et al.*, "A microfabricated atomic clock," Appl. Phys. Lett. **85**, 1460 (2004).
8. Z.-K. Hu, B.-L. Sun, X.-C. Duan, *et al.*, "Demonstration of an ultrahigh-sensitivity atom-interferometry absolute gravimeter," Phys. Rev. A **88**, 043610 (2013).
9. S.-K. Wang, Y. Zhao, W. Zhuang, *et al.*, "Shift evaluation of the atomic gravimeter NIM-AGRb-1 and its comparison with FG5X," Metrologia **55**, 360 (2018).
10. Y. Bidel, O. Carraz, R. Charrière, *et al.*, "Compact cold atom gravimeter for field applications," Appl. Phys. Lett. **102**, 144107 (2013).
11. A. Peters, K.-Y. Chung, and S. Chu, "Measurement of gravitational acceleration by dropping atoms," Nature **400**, 849 (1999).
12. R. H. Parker, C. Yu, W. Zhong, *et al.*, "Measurement of the fine-structure constant as a test of the standard model," Science **360**, 191 (2018).
13. I. Dutta, D. Savoie, B. Fang, *et al.*, "Continuous cold-atom inertial sensor with 1 nrad/sec rotation stability," Phys. Rev. Lett. **116**, 183003 (2016).
14. C. M. Seck, M. G. Kokish, M. R. Dietrich, *et al.*, "Raman sideband cooling of a $^{138}Ba^{+}$ ion using a Zeeman interval," Phys. Rev. A **93**, 053415 (2016).

15. V. M. Porozova, L. V. Gerasimov, I. B. Bobrov, *et al.*, "Raman sideband cooling of a single atom in an optical dipole trap: toward a theoretical optimum in a three-dimensional regime," Phys. Rev. A **99**, 043406 (2019).
16. L. Zhu, Y.-H. Lien, A. Hinton, *et al.*, "Application of optical single-sideband laser in Raman atom interferometry," Opt. Express **26**, 6542 (2018).
17. G. Wang, Y. Wang, K. Ying, *et al.*, "Robust single-sideband-modulated Raman light generation for atom interferometry by FBG-based optical rectangular filtration," Opt. Express **30**, 28658 (2022).
18. J. Mielke, J. Pick, J. A. Coenders, *et al.*, "139 GHz UV phase-locked Raman laser system for thermometry and sideband cooling of $^{9}Be^{+}$ ions in a Penning trap," J. Phys. B **54**, 195402 (2021).
19. D. Hayes, D. N. Matsukevich, P. Maunz, *et al.*, "Entanglement of atomic qubits using an optical frequency comb," Phys. Rev. Lett. **104**, 140501 (2019).
20. J. Mizrahi, C. Senko, B. Neyenhuis, *et al.*, "Ultrafast spin-motion entanglement and interferometry with a single atom," Phys. Rev. Lett. **110**, 203001 (2013).
21. Y. Zhao, S. Wang, W. Zhuang, *et al.*, "Raman-laser system for absolute gravimeter based on ^{87}Rb atom interferometer," Photonics **7**, 32 (2020).
22. P. Cheinet, F. Pereira Dos Santos, T. Petelski, *et al.*, "Compact laser system for atom interferometry," Appl. Phys. B **84**, 643 (2006).
23. S. Lu, Y. Zhou, F. Zhu, *et al.*, "Digital-analog hybrid optical phase-lock loop for optical quadrature phase-shift keying," Chin. Opt. Lett. **18**, 090602 (2020).
24. C. Wei, S. Yan, A. Jia, *et al.*, "Compact phase-lock loop for external cavity diode lasers," Chin. Opt. Lett. **14**, 051403 (2016).
25. A. C. Bordonalli, C. Walton, and A. J. Seeds, "High-performance phase locking of wide linewidth semiconductor lasers by combined use of optical injection locking and optical phase-lock loop," J. Light. Technol. **17**, 328 (1999).
26. P. J. Lee, B. B. Blinov, K. Brickman, *et al.*, "Atomic qubit manipulations with an electro-optic modulator," Opt. Lett. **28**, 1582 (2003).
27. Q. Luo, H. Zhang, K. Zhang, *et al.*, "A compact laser system for a portable atom interferometry gravimeter," Rev. Sci. Instrum. **90**, 043104 (2019).
28. S.-W. Chiow and N. Yu, "Compact atom interferometer using single laser," Appl. Phys. B **124**, 96 (2018).
29. R.-R. Li, R. He, J.-M. Cui, *et al.*, "A versatile multi-tone laser system for manipulating atomic qubits based on a fiber Mach–Zehnder modulator and second harmonic generation," Opt. Express **30**, 30098 (2022).
30. S. Olmschenk, K. C. Younge, D. L. Moehring, *et al.*, "Manipulation and detection of a trapped Yb^{+} hyperfine qubit," Phys. Rev. A **76**, 052314 (2007).
31. E. D. Black, "An introduction to Pound–Drever–Hall laser frequency stabilization," Am. J. Phys. **69**, 79 (2001).